



# Fast photodegradation of Orange II azo dye under visible light irradiation using a semiconducting n–p heterojunction of ZnO nanoparticles/polypyrrole as catalyst

Alondra G. Escobar-Villanueva<sup>1</sup> · Víctor M. Ovando-Medina<sup>1</sup> · Hugo Martínez-Gutiérrez<sup>2</sup> · M. Paula Militello<sup>3</sup>

Received: 18 October 2019 / Accepted: 26 November 2019 / Published online: 2 December 2019  
© Springer Science+Business Media, LLC, part of Springer Nature 2019

## Abstract

Preparation of innovative nano- and microstructured heterojunctions consisting of two semiconductors for highly efficient p–n photocatalysts has been of growing interest due to their advanced applications. n-type ZnO nanoparticles were synthesized by a simple precipitation method from ZnCl<sub>2</sub> and NaOH and coated with semiconducting p-type polypyrrole (PPy) nanospheres by chemical oxidation in the presence of sodium dodecyl sulfate (SDS) as surfactant, obtaining a n-p type ZnO/PPy composite. The composite was characterized by scanning electron microscopy (SEM), FTIR and UV/Vis–NIR spectroscopies, and thermogravimetric analysis (TGA). It was observed that composite consisted of ZnO nanoparticles with rice-like morphology of sizes in the range of 180–600 nm long and between 70 and 227 nm wide, which were well dispersed into a matrix made of agglomerated spherical nanoparticles of PPy. The composite was tested as photocatalyst in the degradation of Orange II azo dye using visible light irradiation at different initial dye concentrations, catalyst loading, initial pH, and in the presence of hole and radical scavengers. Photodegradation efficiencies after 30 min of reaction in the range of 90.9–100% and fast photodegradation rates depending on the initial dye concentration and catalyst load were observed. The best photodegradation efficiency was observed at acidic pH, which was ascribed to an improved electrostatic interaction of dissociated dye molecules with the positively charged surface of photocatalyst. It was demonstrated that ·O<sub>2</sub><sup>-</sup> and other ROS are the main reactive species formed via reaction between O<sub>2</sub> and photogenerated electrons, following a pseudo-first order of reaction.

## 1 Introduction

From food and clothing to cosmetics and drugs, color is the main characteristic of industrialized products [1]. A great amount of synthetic dyes is used in manufacturing processes in industries such as textile, paper, and pharmaceutical, among others [2, 3]. Synthetic dyes are cheap organic

molecules, easy to synthesize, thermally stable, and with more variety in color compared with natural dyes [4]. Their colors are due to the presence of chromophores chemical groups that absorb light in the visible spectrum, for example, the azo dyes which contain the N=N chemical group [5, 6].

A growing environmental problem is the high concentration of dyes in effluents from industrial application, because only a small percentage of the dye in the solutions is really attached to cloths, and the remaining dye is discarded without any treatment. The problem is increased considering that some dyes are toxic and recalcitrant [7] and non-conventional technologies must be used for their treatment, because conventional processes only change the pollutant present in a high volume of water to a small surface (adsorption) or cumulate dye in relatively smaller volumes (i.e., coagulation and filtration), thus the pollution persist [8–10].

Therefore, it is necessary to develop new technologies with advanced materials but increasing its recyclability and efficiency. One option for this purpose is the photocatalysis, which can mineralize organic recalcitrant dyes or, when total mineralization is not achieved, this process can reduce the

✉ Víctor M. Ovando-Medina  
ovandomedina@yahoo.com.mx

✉ Hugo Martínez-Gutiérrez  
hmartinez63@hotmail.com

<sup>1</sup> Chemical Engineering, COARA – Autonomus University of San Luis Potosi, Road to Cedral KM 5+600, 78700 Matehuala, San Luis Potosi, Mexico

<sup>2</sup> Instituto Politécnico Nacional-CNMN, Luis Enrique Erro S/N, 07738 Mexico City, D.F, Mexico

<sup>3</sup> Instituto de Investigaciones en Tecnologías Energéticas y Materiales Avanzados (IITEMA), Universidad Nacional de Río Cuarto (UNRC) – CONICET, 5800 Río Cuarto, Córdoba, Argentina

pollutant dyes to non-toxic products by using photoactive materials such as  $\text{TiO}_2$  and  $\text{ZnO}$  [11–14]. The advantage of  $\text{ZnO}$  over  $\text{TiO}_2$  in photocatalytic applications is that  $\text{ZnO}$  presents a wider light adsorption band in the solar spectrum [15]. However, its reported band gap is higher than that of  $\text{TiO}_2$ .  $\text{ZnO}$  is an important n-type semiconductor with interesting properties, for example, it has wide band gap energy (between 3.2 and 3.4 eV), shows wide absorption of light mainly in the UV region (high photoactivity), large exciton binding energy (60 meV), physical and chemical stability, biocompatibility, and has relatively low toxicity [16, 17]. It has been considered as a promising photocatalyst that can degrade different recalcitrant contaminants under UV light, which accounts only 3–5% of the total sunlight irradiation reaching the Earth's surface [18]. Therefore, it is necessary to develop visible-light-activated catalysts in order to exploit a higher portion of the solar spectrum, especially the visible region because it represents approximately 40% of the sunlight at the Earth's surface and it is easier and safer to work with.  $\text{ZnO}$  nanoparticles show improved performance in comparison to bulk  $\text{ZnO}$  due to increased superficial area, shorter diffusion length, and high light absorption [19]. Different studies about the preparation of  $\text{ZnO}$  nanoparticles and its composites can be found in literature, for instance, Hassanein et al. [20] developed a sensor based on chitosan,  $\text{ZnO}$  nanoparticles and PPy, and was used for isoxsuprine-HCl quantification. They observed a significant improvement in electrical conductivity of nanocomposite by increasing the chitosan percentage. Almuntaser et al. [21] built a solar cell based on fluorine-doped tin oxide/PPy/polythiophene/ $\text{ZnO}/\text{Al}$ . They studied the effect of PPy active layer thickness on the device performance. Kant et al. [22] fabricated  $\text{ZnO}$  nanostructured thin films to be used as photoanodes for photoelectrochemical water splitting. They used Al-doped  $\text{ZnO}$  seed layers as template to grow  $\text{ZnO}$  nanostructures and studied the applied voltage during the spray on the photoelectrochemical properties of  $\text{ZnO}$  nanostructures.

To shift the  $\text{ZnO}$  photoactivity towards the visible light region, Chen et al. [23] reported the synthesis of macroporous zinc oxide (c- $\text{ZnO}$ ) and  $\text{Au}/\text{c-}\text{ZnO}$  photocatalysts using hydrothermal and electrostatic self-assembly methods. These photocatalysts, c- $\text{ZnO}$  and  $\text{Au}/\text{c-}\text{ZnO}$ , exhibited good photodegradation efficiency of Orange II dye, however, they reached only between 82 and 87% of photodegradation efficiency after 3 h of UV light irradiation, and 99% of efficiency after 10 h of visible light irradiation. In another work, Mohd Hir et al. [24] reported a technique to immobilize  $\text{ZnO}$  nanoparticles on polymeric membranes of poly(ether-sulfone) fabricated by phase inversion method. The resultant  $\text{ZnO}/\text{polymer}$  composites films (units of  $10 \times 8$  cm) were tested in the degradation of methyl orange dye. They observed that photocatalytic performance increased with the number of film units immersed into the dye solutions.

In the present work, n–p type heterojunction of  $\text{ZnO}/\text{PPy}$  composite was synthesized polymerizing pyrrole monomer by chemical oxidation in the presence of sodium dodecyl sulfate (SDS) as surfactant onto  $\text{ZnO}$  nanoparticles of rice-like morphology previously obtained by a simple precipitation reaction route with high reproducibility. The composite was tested as photocatalyst in the fast degradation of Orange II azo dye (Fig. 1) under visible light irradiation at different catalyst loading, initial dye concentrations, and pH, achieving photodegradation efficiencies as high as 100% in only 30 min of light irradiation and showing very good reusability and chemical stability under the studied conditions, thus, decreasing the costs of these wastewater treatment processes. The main reactive species were identified by dye photodegradation experiments in the presence of different hole and radical scavengers.

## 2 Experimental

### 2.1 Materials

Pyrrole (> 98%), ammonium persulfate (APS > 98%), and Orange II (dye content  $\geq 85\%$ ) were acquired from Sigma-Aldrich and used as received.  $\text{ZnCl}_2$  (99%) and  $\text{NaOH}$  (98.9%) were purchased from Jalmeq (San Nicolas de los Garza, Mexico). Sodium dodecyl sulfate (SDS > 98%) was acquired from HYCEL (Guadalajara, Mexico). Deionized grade water was used in the experiments.

### 2.2 $\text{ZnO}/\text{PPy}$ composite synthesis

$\text{ZnO}$  nanoparticles were synthesized as previously reported [25] by precipitation from aqueous solution of  $\text{ZnCl}_2$  but controlling the  $\text{NaOH}$  solution addition rate. Concisely, a zinc chloride solution consisting 8.20 g of  $\text{ZnCl}_2$  in 60 mL of water was mixed with an SDS solution (0.86 g of SDS in 15 mL of water) under magnetic stirring at 70 °C. Then, a  $\text{NaOH}$  aqueous solution (14.4 g of  $\text{NaOH}$  in 90 mL of water) was dosed to reaction mixture using an addition pump (KdScientific) at a rate of 3.0 mL/min with magnetic

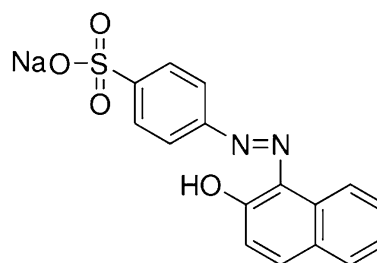


Fig. 1 Chemical structure of Orange II azo dye

stirring. Subsequently, 135 mL of distilled water was added to reaction mixture, and reaction was allowed to proceed for 1.5 h. After that, the reaction mixture was poured in a 500-mL screw-top glass jar, sealed and placed in an oven at 80 °C for 5 h. ZnO product was formed at the bottom of the container, and the supernatant solution was decanted. ZnO nanoparticles were washed with hot water and dried at 60 °C by 24 h.

The synthesis of ZnO/PPy composite was as follows: 2.0 g of synthesized ZnO was well dispersed with ultrasound by 15 min in 100 mL of water and 2.0 g of SDS. Subsequently, 2.0 g of pyrrole monomer was added and stirred for 2 h to allow the pyrrole adsorption over ZnO nanoparticles. Then, 6.8 g of APS was added to start polymerization, which proceeded by 2 h. Afterwards, the mixture was filtered and washed with hot water to remove unreacted substances and dried at 60 °C by 24 h.

### 2.3 Characterization

ZnO and dried composites were analyzed by FTIR spectroscopy (Agilent, Cary 630). Scanning electron microscopy was made (JEOL HRSEM, JSM 7800F at 30 kV of beam acceleration) dispersing samples in deionized water and sonicated. A drop of the dispersed sample was transferred to a copper grid covered with Formvar™ resin and carbon film and dried at room temperature. Elemental analysis was made by Energy Dispersive X-Ray Spectroscopy with a detector coupled to the electronic microscope. The composite was also analyzed by UV/Vis–NIR diffuse reflectance spectroscopy measured between 200 and 800 nm using a spectrophotometer (Thermo Scientific, Evolution 220) equipped with an integrating sphere. Thermal stability of samples was studied by thermogravimetric analysis (TGA550, TA Instrument) using 10 mg of sample heated from 25 to 450 °C at a heating rate of 20 °C/min. ZnO and ZnO/PPy composite were analyzed in a PANALYTICAL Empyrean diffractometer, equipped with a copper K $\alpha$  source. Diffraction patterns were obtained at 2.7°/min of scanning rate and a step of 0.026°.

### 2.4 Electron–hole pair photogeneration test

Iodide ion ( $I^-$ ) act as scavenger of photogenerated holes at the surface of a photocatalytic material. In the presence of holes,  $I^-$  is oxidized to triiodide ( $I_3^-$ ), and while  $I^-$  does not show any absorption band in the UV/Vis spectrum, triiodide has two well-defined adsorption bands at 286 nm and 345 nm, respectively [26]. Therefore, 100 mL of potassium iodide (KI) aqueous solution (0.06 N) was mixed with 0.1 g of composite and ultrasonicated by 5 min. Afterwards, sample was exposed to a visible light source (halogen lamp) under magnetic stirring, taking samples at different intervals

of time and analyzed in a UV/Vis spectrophotometer to determine their absorbance spectra.

### 2.5 Photocatalytic performance of ZnO/PPy composite

ZnO/PPy composite was tested in Orange II (OII) dye photodegradation in aqueous solutions. The reactor consisted of a glass container with two quartz compartments (Figure S1 in the Electronic Supplementary Information), the first for reaction mixture cooling, and the second for the visible light source insertion (halogen lamp, Philips H7, 55 W, with emission between 350 and 1200 nm of wavelength and a maximum irradiance of 1.5  $\mu\text{W}/\text{cm}^2$  [27]). 75, 100, and 150 mg of ZnO/PPy composite (0.5, 0.67, and 1.0 g/L, respectively) were used in OII photodegradation experiments. The composite was sonicated in 5 mL of water and added to 0.15 L of OII dye aqueous solution at 20 mg/L of initial concentration. The pH of solution was adjusted adding NaOH or HCl 0.1 N. Reaction mixtures were exposed to the visible light source to start photodegradation. Samples of approximately 1.5 mL were taken and centrifuged to separate solids and determine the absorbance by UV/Vis spectroscopy (Thermo Scientific, Evolution 220) at a wavelength of 485 nm to calculate the remaining dye concentrations with respect to the absorbance of initial dye solution. In addition, initial OII dye concentrations were changed to 10 and 40 mg/L when working with the ZnO/PPy composite at a fixed concentration of 1.0 g/L (0.15 g of composite).

OII photodegradations using ZnO/PPy composite were also carried out in the presence of KI and methanol as hole and radical scavengers, respectively, using 150 mL of OII dye solution at 20 mg/L with 0.15 g of composite and in the presence of KI 0.06 N, methanol 1 M, or bubbling the reaction mixture with  $N_2$ . Photolysis was determined in similar photodegradation conditions but without composite, whereas physical dye adsorption was determined with composite but in the darkness. Reusability of composite was determined recovering the ZnO/PPy after photodegradation by filtration, washing, and drying at 80 °C and used again in a photodegradation at 20 mg/L of initial dye concentration and 0.15 g of composite, the test was repeated by 5 cycles.

### 2.6 Open circuit potential measurements

Photoelectrochemical measurement (open circuit potential, OCP) was performed using a potentiostat/galvanostat (GAMRY, G300) coupled to a cell filled with 200 mL of 0.5 M NaOH as electrolyte. The cell was equipped with three electrodes: a working electrode made of the ZnO/PPy composite deposited on glass previously coated with a graphite film with a size of 1.5 cm  $\times$  1.5 cm, an electrode of Ag/AgCl as the reference, and a platinum net as the counter electrode,

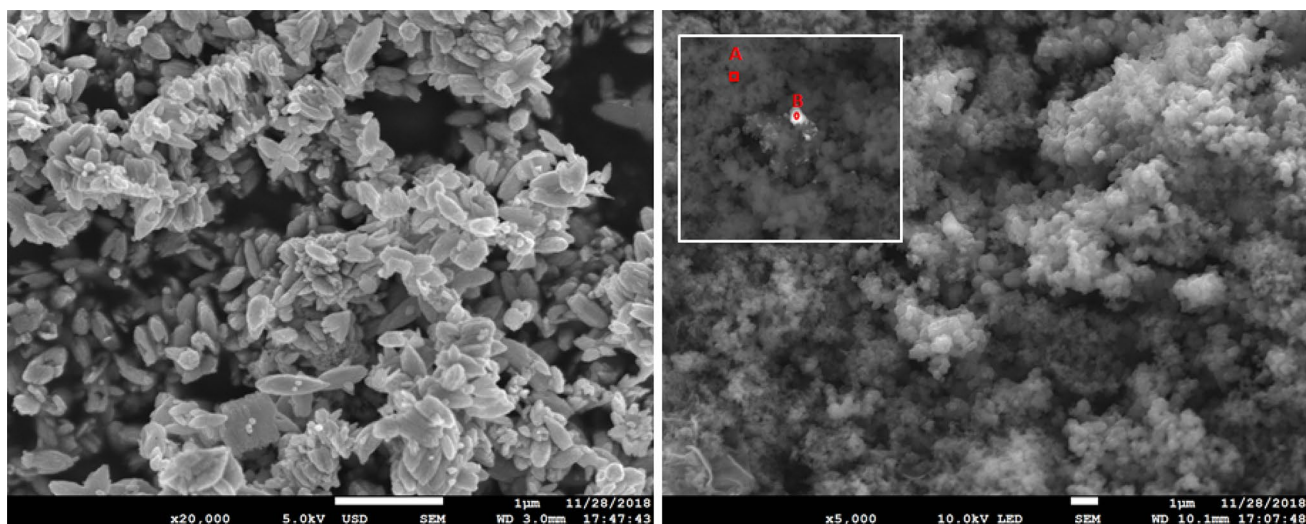
respectively. Experiments in the dark were made covering the cell with a box, while the experiments with illumination were made using a LED light bulb of 50 W (Philips, LED 6500 K 110-130 V).

### 3 Results and discussion

Figure 2a shows the SEM image of ZnO nanoparticles synthesized in this work where a rice-like morphology can predominantly be observed. The sizes of these nanoparticles were in the range from 70 to 227 nm wide and between 180 and 600 nm long; counting 400 particles (ImageJ software™), the number-average width was  $96 \pm 5$  nm and the length was  $206 \pm 7$  nm, respectively. From Fig. 2b, it can be observed a composite made of ZnO nanoparticles inserted in a matrix of semiconducting polypyrrole of spherical morphology. We have previously reported the synthesis of ZnO by the methodology here used but at room temperature and without control of the NaOH addition rate, where morphologies of the ZnO microparticles of six-blade impeller and cabbage-like were usually obtained [25]. In the present work, the ZnO synthesis was made at 70 °C instead of at room temperature and with addition rate of the NaOH solution at 3 mL/min. Then, different morphology and sizes were obtained. It has been reported that ZnO morphology can be strongly affected by the synthesis conditions like alkali type, concentration, addition mode (batch or continuous), temperature, stirring rate, surfactants, etc. For example, Xie et al. [28] reported the synthesis of ZnO of morphologies as needle-like, rod-like or rugby-like, depending on the surfactant, alkali type (NaOH or LiOH), and alkali concentration used

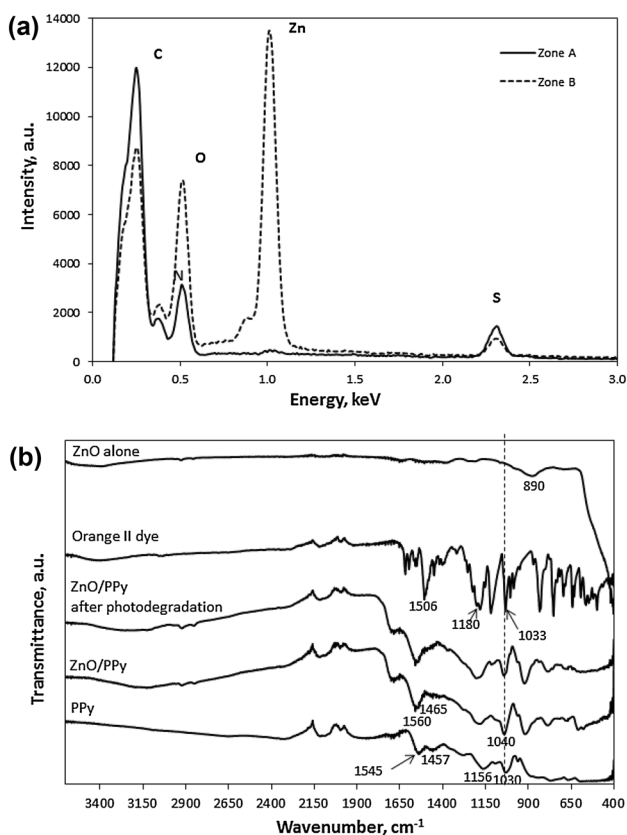
in the synthesis, which resulted in different photodegradation efficiencies of methyl orange dye.

Figure 3a shows the elemental analysis obtained by EDS made in two different zones of the SEM image (shown as square and circle in Fig. 2b, respectively). It can be seen in Fig. 3a that sample in the circle is composed by a higher content of ZnO, whereas that in the square corresponds to organic material (PPy rich: C and N). These results demonstrate the presence of well-dispersed ZnO nanoparticles in the semiconducting polypyrrole matrix. Additionally, in both EDS spectra from Fig. 3a, sulfur is observed, which indicates that some surfactant and oxidizing agent remained after composite washing. Figure 3b shows the FTIR spectra of ZnO nanoparticles, PPy alone, Orange II dye, and the ZnO/PPy composite before and after dye photodegradation, respectively. It can be observed from the ZnO spectrum the typical signal of ZnO interaction in stretching mode near to  $890\text{ cm}^{-1}$  [29]. The PPy spectrum exhibited the characteristic signals of this polymer at  $1545\text{ cm}^{-1}$  which is shifted to  $1560\text{ cm}^{-1}$  when the ZnO is present in the composite, indicating a chemical interaction between PPy and ZnO. The weak band at  $1457\text{ cm}^{-1}$  assigned to stretching vibration of C=C and C–C in the pyrrole units was also moved to  $1465\text{ cm}^{-1}$  for the composite. The peak corresponding to ZnO in the composite spectra is not present due to PPy chains coating ZnO nanoparticles. In the FTIR spectrum of OII dye, the weak band at  $1033\text{ cm}^{-1}$  corresponds to the –N=N– bond stretching vibration, and the band at  $1180\text{ cm}^{-1}$  is assigned to the –C–O– bond stretching vibration [30]. These two signals were not observed in the recovered composite after a photodegradation, indicating that even when adsorption was present, dye molecules were fully degraded as will be discussed later.



**Fig. 2** Micrography of **a** synthesized ZnO nanoparticles and **b** composite of ZnO/PPy. The inset corresponds to a section of the same SEM image with contrast. A and B describe the zones of the sample where EDS analyses were made





**Fig. 3** **a** EDS spectra of ZnO/PPy composite. A and B represent the zone of SEM image where EDS analysis was made. **b** FTIR spectra of ZnO nanoparticles, OII dye, alone PPy, and ZnO/PPy composite before and after photodegradation experiments

Figure 4a shows the UV/Vis spectra of ZnO nanoparticles and composite. ZnO nanoparticles presented a high absorption peak in the ultraviolet region with wavelength in the range of 250–400 nm with a maximum at 300 nm, which

agrees with that reported in the literature [25]. Also, the ZnO/PPy composite presented broader photoactivity than the ZnO nanoparticles, not only in the UV region but also in the visible region with the absorption edge shifted towards higher wavelengths values, which is due to the presence of the semiconducting PPy. Two absorption bands with maxima at 475 nm and 900 nm were observed for the composite. The first is attributed to transitions of the valence band to the polaron state, which is related to PPy chain conductivity (interactions  $\pi$ -bonding/ $\pi$ -antibonding), while the second peak is due to bipolaron state, and can be ascribed to the presence of remaining molecules used in the synthesis, for example, surfactant or APS physically attached to composite, acting as dopants [29].

For photocatalysis purposes, electrons of the semiconducting material must be excited from the valence band to the conducting band with photons of enough energy which is called band gap energy [31]. The lower the band gap value, the easier the electrons are promoted, in other words, low energy light as the visible can accomplish the photocatalytic process. The inorganic material of reference is TiO<sub>2</sub> due to its low band gap energy (3.0 eV for rutile and 3.2 eV for anatase phases, respectively), however, it is photoactive only under the UV light. The band gap energy calculated by intersection of the linear section of Kubelka–Munk data with the straight-baseline of Fig. 4b was 3.05 eV, which is slightly lower than that previously reported for ZnO particles but synthesized at room temperature [25]. The band gap value of ZnO/PPy composite was not possible to determine due to the absorbance spectrum shown but it is enough to observe its wide photoactivity in the part of the UV and all the visible region of the electromagnetic spectrum. It was observed from the XRD analysis (Electronic Supplementary Information, Figure S2) that ZnO showed the typical peaks of hexagonal wurtzite crystals, while the composite showed

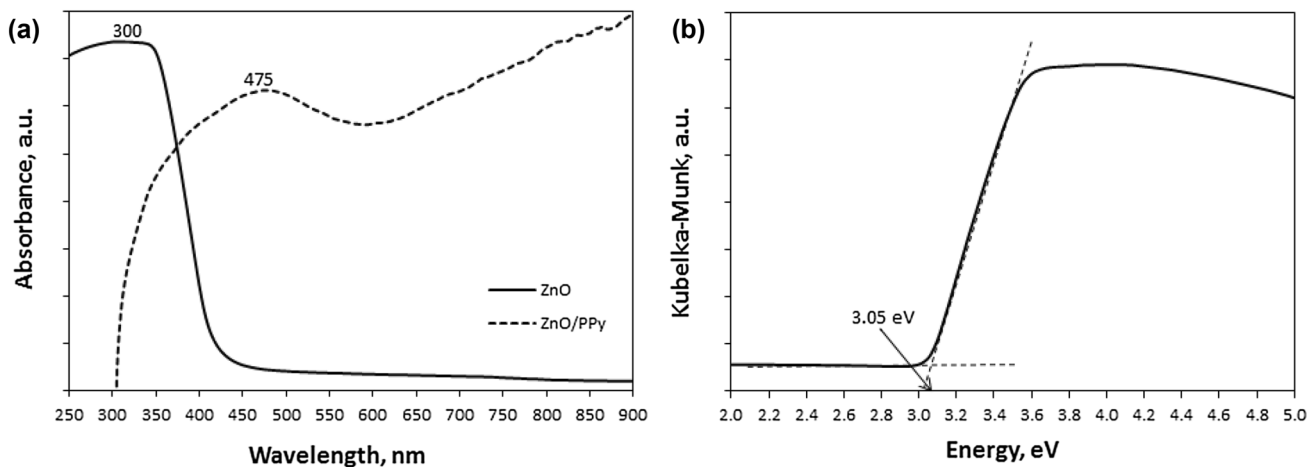


**Fig. 4** **a** UV/Vis–NIR spectra of ZnO nanoparticles and ZnO/PPy composite, and **b** Kubelka–Munk of ZnO nanoparticles

the ZnO signals with less intensity and the characteristic amorphous behavior of PPy with a wide peak of crystallinity between 15 and 30° of  $2\theta$ .

Thermal stability of samples was determined by TGA as can be seen in Fig. 5a and b. It can be observed that uncoated ZnO nanoparticles showed only a weight loss of about 2.3% which can be ascribed to water physically absorbed, while alone PPy and ZnO/PPy composite presented similar behavior with two important changes, the first centered at 172 °C and the second at 300 °C for alone PPy; this second temperature change was shifted to 310 °C in the composite, indicating higher thermal stability due to decreased PPy chain mobility in the presence of ZnO inorganic nanoparticles.

Holes ( $h^+$ ) photogeneration in the surface of ZnO/PPy composite under visible light irradiation was demonstrated by the reaction of  $I^-$  ions with  $h^+$  giving triiodide ions. Figure 6 shows the UV/Vis spectra of KI aqueous solution in the presence of ZnO/PPy composite at different times of visible light irradiation. Initial sample of KI solution did not present absorbance bands, while samples after visible light exposition showed the two mentioned absorption bands but centered at 288 nm and 350 nm increasing continuously their intensity indicating the triiodide ion formation due to  $h^+$  photogeneration. In our previous paper [26], where a similar ZnO/PPy composite was studied but with the difference that ZnO in the microscale was obtained, the triiodide ion formation increased continuously until 30 min of visible light exposition, and then started to decrease and increased again at 90 min of reaction. This behavior can be due to  $e^-/h^+$  pair recombination to some extent, which was not observed in the present work, and then would be expected an improved photocatalytic performance.

ZnO/PPy composite was tested in the Orange II dye photodegradation in aqueous solutions under visible light

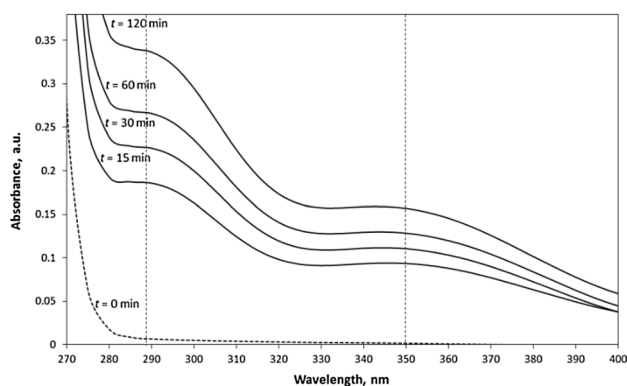


**Fig. 6** UV/Vis spectra of KI aqueous solution in the presence of ZnO/PPy composite under visible light irradiation at different intervals of time

irradiation. Figure 7 shows the UV/Vis spectra of OII dye aqueous solutions at different times. Solutions were prepared employing an initial OII dye concentration of 10 mg/L and 0.15 g of ZnO/PPy composite load. Figure 7 highlights the positive effect of PPy on the photocatalytic activity of alone ZnO under visible light (Fig. S3 of Electronic Supplementary Information). A fast decrease of the intensity of the peak at 485 nm can be observed after only 1 min of photodegradation with the visible light irradiation corresponding to approximately 76% of photodegradation efficiency, reaching 98.7% of efficiency after 10 min of reaction until almost 100% in 30 min. The inset in Fig. 7 is a photography of centrifuged samples at different times of reaction, where a total discoloration of solution after 10 min of reaction can be appreciated.

Based on the above results, photodegrading kinetics studies were made considering 30 min of reaction.

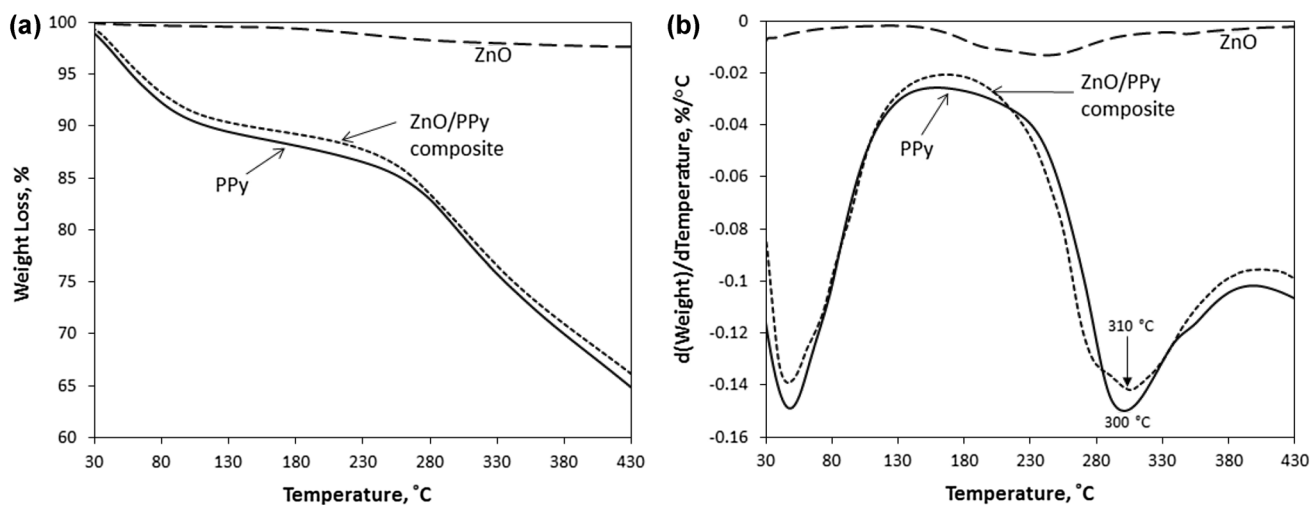


**Fig. 5** **a** Thermogram and **b** derivative of ZnO, ZnO/PPy composite, and alone PPy, respectively

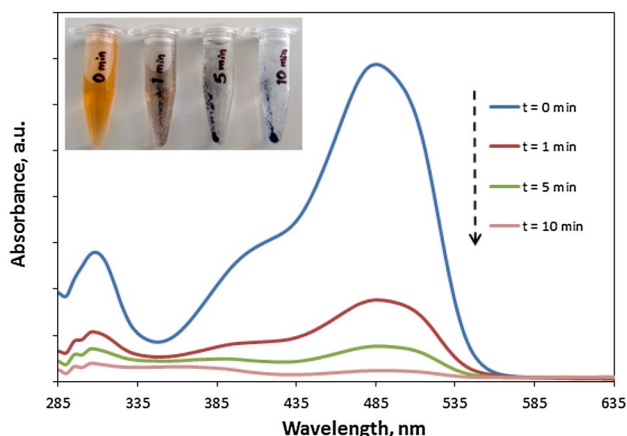


**Fig. 7** UV/Vis spectra profile of OII dye photodegradation at 10 mg/L of initial dye concentration and 0.15 g of ZnO/PPy composite under visible light irradiation

Figure 8a shows the ratio of residual to initial OII dye concentration ( $C/C_0$ ) kinetics using 0.15 g of ZnO/PPy composite (1.0 g/L) for different OII initial concentrations. As discussed, practically 100% of degradation efficiency can be obtained after only 30 min of light exposure for 10 mg/L of OII of initial concentration, however, by increasing twice the initial dye concentration to 20 mg/L keeping constant the catalyst load at 1.0 g/L, degradation efficiency decreased only to 95.5%; moreover, increasing fourfold OII dye initial concentration, still acceptable efficiency was observed (92.5%). It is of importance to observe in the FTIR spectrum of ZnO/PPy composite after photodegradation test, shown in Fig. 3b, that bands of the Orange II dye are not present in the composite,

demonstrating that physical adsorption is not present at the end of experiment, and discoloration of solutions are effectively due to the radicals produced by the reaction of photogenerated holes at the surface of composite with water and reaction of photogenerated  $e^-$  with dissolved oxygen. Figure 8b shows the effect of ZnO/PPy composite load on the OII dye photodegradation kinetics with a fixed initial OII dye concentration (20 mg/L). Decreasing the amount of ZnO/PPy to 66% (from 0.15 to 0.10 g), and after 30 min of reaction, only a decrease in degradation efficiency of 2.6% was observed; while reducing to 50% the amount of ZnO/PPy composite, the degradation efficiency dropped to 90.9%, thus the photocatalyst amount or initial dye concentration does not affect significantly the photodegradation efficiency under the studied conditions.

When the reaction order of photodegradation mechanism ( $OII + \text{radical oxygen species} \rightarrow \text{products}$  from the reaction of photogenerated  $e^-$  and dissolved oxygen, or  $OII + \cdot OH \rightarrow \text{products}$  from the reaction of  $h^+$  and water) follows a pseudo-first-order mechanism, the following equation is valid:

$$-\frac{dC}{dt} = kC, \tag{1}$$

where  $t$  represents the photodegradation time (min) and  $k$  ( $\text{min}^{-1}$ ) is the observed pseudo first-order rate constant. By integrating Eq. 1, the following expression is obtained:

$$-\ln\left(\frac{C}{C_0}\right) = kt. \tag{2}$$

Photodegradations were well described by the pseudo first-order model, in other words, the photodegradation

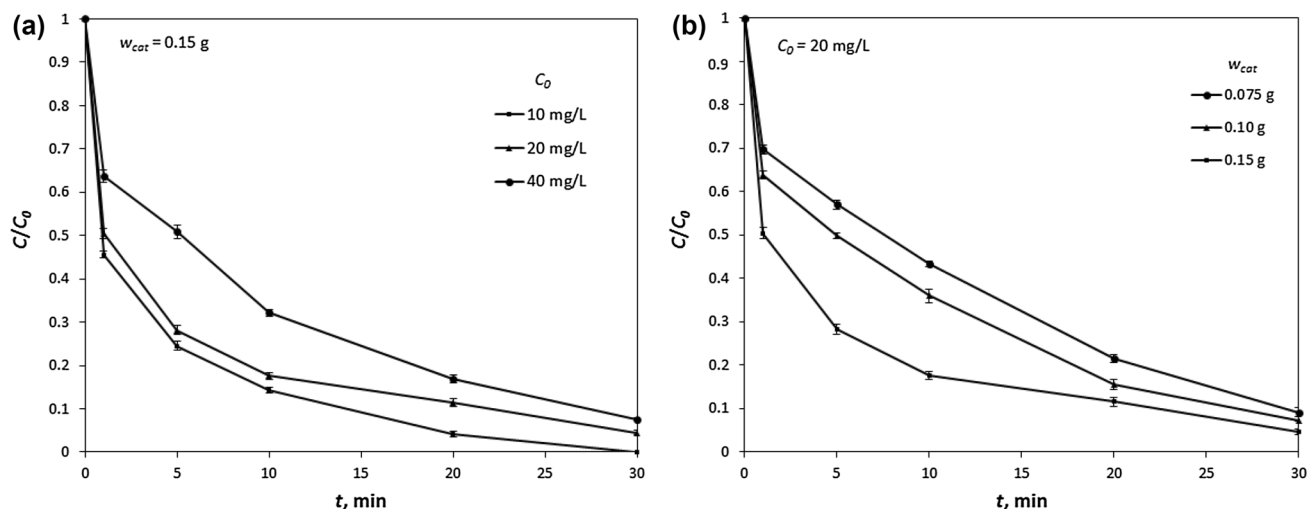


**Fig. 8**  $C/C_0$  kinetics in the OII dye photodegradation experiments under visible light irradiation using the ZnO/PPy composite as photocatalyst. **a** At different dye initial concentrations **b** at different catalyst loads

rates are proportional to OII dye concentration (Fig. 9). Table 1 shows the calculated  $k$  values.

Achouri et al. [32], who employed porous ZnO nanoparticles doped with Mn for solar and visible light OII photodegradation, achieved only 60–95% of degradation efficiency after 240 min for dye solutions in concentrations between 10 and 20 mg/L. Benaboud et al. [33] synthesized  $\text{Fe}_2\text{O}_4/\text{ZnO}$ -nanowires for OII photodegradation under visible light irradiation, obtaining a decolorization efficiency of 42% within approximately 6 h in similar conditions of dye concentrations and catalyst load. Furthermore, Zhang et al. [34] improved the photocatalytic efficiency of ZnO by doping with bismuth oxybromide, reaching 90% of OII dye degradation of a 20 mg/L dye solution after 60 min of reaction. Other authors also focused on this dye solutions as industrial wastewater model and reported works in similar reaction conditions and under visible light irradiation, using catalysts based on  $\text{TiO}_2$ . For example, Balta et al. [35] employed carbon fiber and  $\text{WO}_3/\text{TiO}_2$  composite catalysts to photodegrade OII dye and achieved 98% of efficiency after 3 h, but only about 60% in 30 min. Zr-doped  $\text{TiO}_2$ /chitosan composite showed enhanced visible light-mediated photoactivity for the degradation of OII dye; the presence of chitosan increased the removal efficiency of the catalysts from 45% to almost 100% under UV light but only 84% under visible light after 180 min of irradiation [36, 37]. These results somehow highlight the high efficiency of removal, in terms of photodegradation percentage and required time of reaction, of the catalysts reported in the present work.

In the previous photodegradation experiments, dye solutions presented an initial pH of approximately 7.4. Therefore, more experiments were made at acidic and alkaline pH of 3.0 and 9.0, respectively. The comparisons are shown in Fig. 10a. Faster photodegradation rate and higher efficiency

**Table 1** First-order  $k$  values determined from  $-\ln(C/C_0)$  versus time data through OII dye photodegradation

Run	$C_0$ , mg/L	$W_{\text{cat}}$ , g	$C_{\text{cat}}$ , g/L	$k$ , $\text{min}^{-1}$
1	10	0.150	1.00	0.1256
2	20	0.150	1.00	0.0764
3	40	0.150	1.00	0.0737
4	20	0.100	0.67	0.0766
5	20	0.075	0.50	0.0703

at acidic pH (99%) can be observed, while at alkaline pH the efficiency decreased to 53% after 30 min of visible light irradiation. The improved efficiency at acidic pH is a consequence of the enhanced electrostatic interaction between the composite surface and dissociated dye molecules. According to the point of zero charge (PZC) diagram (Fig. 10b), the surface of the composite is positively charged (in the average) at pH below 3.5 and negatively charged above this value. Herrera et al. [38] determined the speciation diagram of the OII dye using two  $\text{p}K_A$  values, the first  $\text{p}K_{A1}$  at 11.4, which belongs to naphthalene-OH group ionization, and a  $\text{p}K_{A2}$  of 1.0 corresponding to  $-\text{SO}_3\text{H}$  group of OII dye ionization; therefore, at different pH values of dye solution, the neutral (HL) and two forms of dissociated OII dye can be present (one and two ionizations:  $\text{HL}^-$  and  $\text{L}^{2-}$ ). They observed that at  $\text{pH} > 12$ , only the negative  $\text{L}^{2-}$  exists in the solution. The ionic species the  $\text{HL}^-$  coexist in solution with  $\text{L}^{2-}$  at pH between 8 and 12. At  $\text{pH} < 8$ , the dye exists mainly as  $\text{HL}^-$ . Then, photodegradation at alkaline pH implies that dye molecules are doubly negatively ionized, and the composite surface is negatively charged according to PZC diagram, subsequently a high electrostatic repulsion is present, diminishing photodegradation efficiency near to

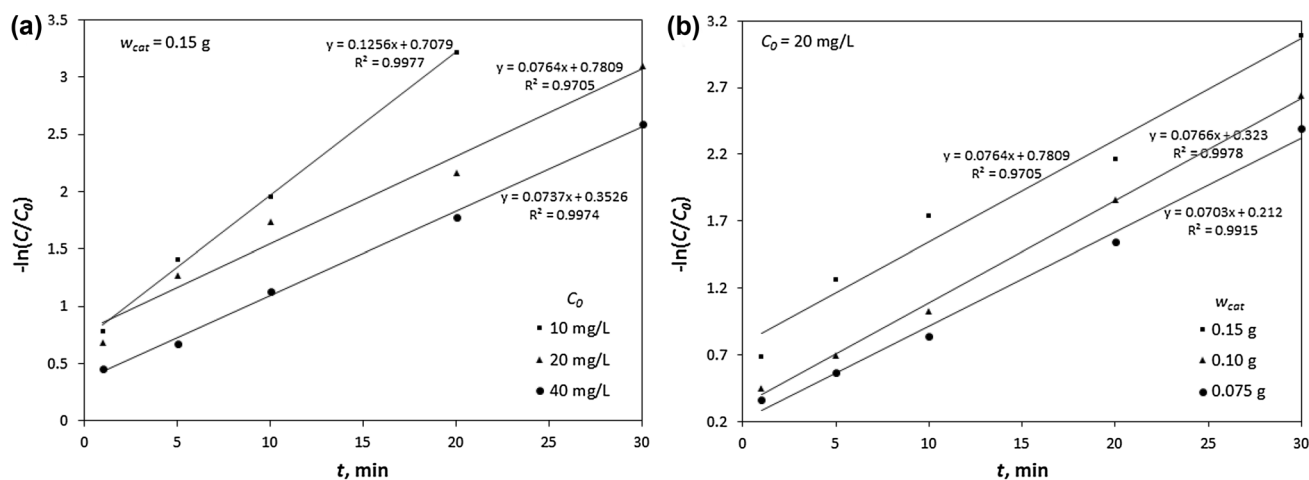


**Fig. 9**  $\ln(C/C_0)$  profiles in the OII dye photodegradations using ZnO/PPy composite as catalyst. **a** At different initial dye concentrations **b** at different catalyst loads



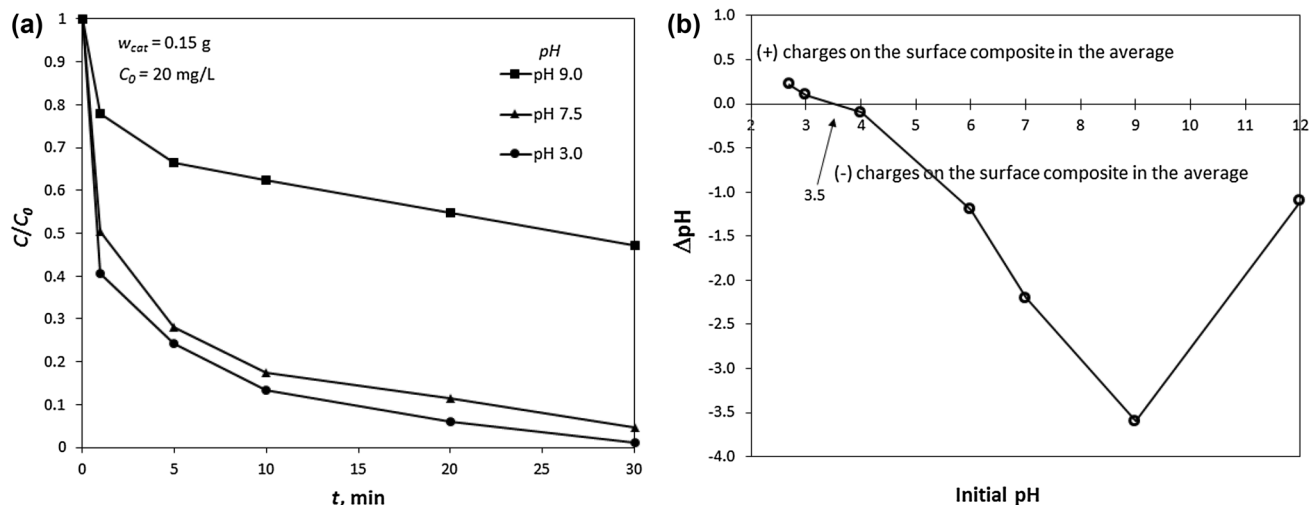


**Fig. 10** **a** Kinetics of OII dye photodegradation under visible light irradiation using ZnO/PPy composite at different solution pH. **b** Point of zero charge diagram of composite

the composite surface, and the observed photodegradation efficiency at alkaline pH is due to photogenerated radicals diffusing until the bulk solution. Contrary, at acidic pH, the positively charged surface of composite strongly attracts the negatively charged dye molecules ( $\text{HL}^-$ ) favoring the photodegradation at the surface of composite.

From an economic point of view, reusability of composite without significant efficiency loss is an important feature. To determine the reusability of the synthesized composite, this was recovered after photodegradations at 20 mg/L of initial dye concentration and 0.15 g of composite by filtration, washed with hot water, dried at 80 °C, and used again in a similar photodegradation test; the process was repeated for 5 cycles. The results of the efficiency after 30 min of reaction for the 5 cycles are shown in Fig. 11. It can be seen a high stability of the composite because efficiency decreased only 1.33% after the cycle #5. It has been reported that decrease of photodegradation efficiency is usually due to formation of organic contaminants or carbon deposition on the surface of catalyst [39]. In the present study this behavior was not observed, demonstrating the economic feasibility of composite under the studied conditions.

Different works have proposed the photodegradation mechanism in the presence of inorganic/organic composite materials used as photocatalyst where the organic material acts as a photosensitizer or co-catalyst. If only the inorganic photocatalysts such as semiconducting  $\text{TiO}_2$  or ZnO are used, the photodegradation mechanism starts when a photon with enough energy reaches the surface of catalyst, promoting electrons from the valence band (VB) to the conduction band (CB). Consequently,  $h^+$  are generated in the VB of semiconductor, which react with water producing  $\cdot\text{OH}$  radicals, while the promoted electrons to

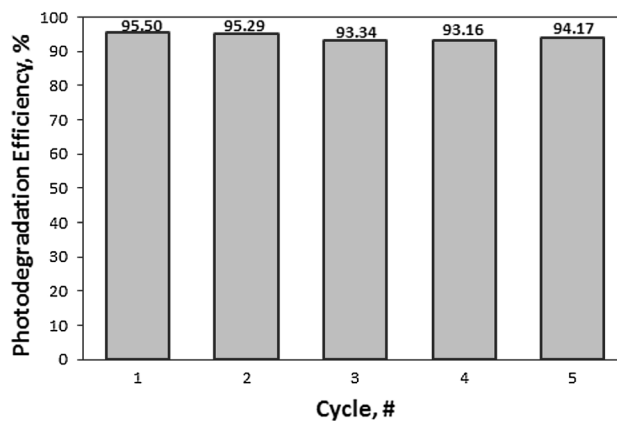


**Fig. 11** Photodegradation efficiency of OII dye under visible light irradiation using ZnO/PPy composite for different cycles using the recovered composite

the conduction band can react with dissolved oxygen giving radical oxygen species (ROS) such as superoxide or singlet oxygen, which can degrade organic matter such as dye molecules until mineralization [40]. In the case of  $\text{TiO}_2/\text{PPy}$  or ZnO/PPy composites, it has been proposed that photons of enough energy reaching the composite surface of PPy, pull-out from the highest occupied molecular orbital (HOMO) and send it to the lowest unoccupied molecular orbital of this conducting polymer, extracted electrons are sent to the conduction band of the inorganic semiconducting material, in this case the ZnO, generating  $h^+$  in the HOMO of PPy. Electrons in the VB of ZnO move to the HOMO of PPy to recombine with these holes and, at the same time, highly reactive  $h^+$  are generated in the VB of ZnO [28, 41].

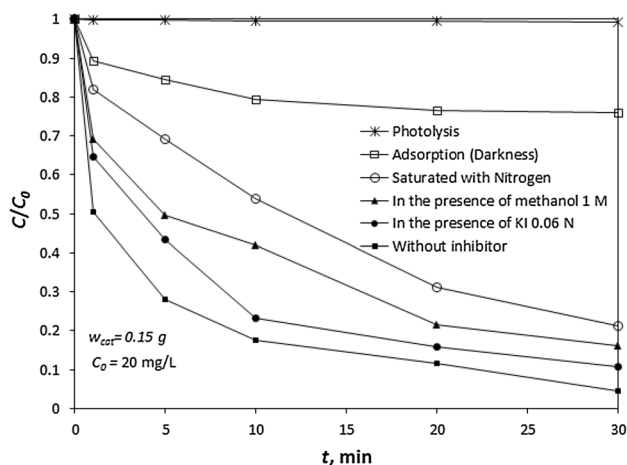


**Fig. 12**  $C/C_0$  as a function of time throughout OII dye photodegradation under visible light irradiation using ZnO/PPy composite in the presence of different inhibitors

To differentiate the photodegradation mechanism, reactions were carried out in the presence of KI as  $h^+$  scavenger, methanol as  $\cdot\text{OH}$  radical scavenger or  $\text{N}_2$  was bubbled to displace dissolved oxygen to avoid ROS formation by reaction of  $e^-$  with  $\text{O}_2$ . Figure 12 shows the photodegradation kinetics of OII dye under visible light irradiation for 20 mg/L of initial dye concentration with 0.15 g of ZnO/PPy composite in the presence of the mentioned inhibitors, as well as without inhibitor but in the darkness to determine the physical dye adsorption, and the dye photolysis (without catalyst). Visible light by itself (photolysis) did not significantly degrade OII dye, which was comparable to the photodegradation observed when using alone ZnO (Electronic Supplementary Information, Figure S3). However, physical dye adsorption represents 26% of water discoloration. As shown in the FTIR results, the signals of OII dye were not observed, thus even when physical adsorption was present, dye molecules were degraded. It can be also observed that the presence of KI through photodegradation diminishes the efficiency from 95.5 to 89.2% and methanol presence decreased efficiency to 83.8%, while the  $\text{O}_2$  absence resulted in photodegradation efficiency to 78.7%. Then, it can be concluded that although both radical generation mechanisms are present,  $\cdot\text{O}_2^-$  could be the main reactive species formed via reaction between  $\text{O}_2$  and electrons under the studied conditions.

To understand the photoactivity of the synthesized ZnO/PPy composite, the photoelectrochemical characterization was performed supporting the composite on a conductive glass/graphite film. Figure 13 shows the variation of the OCP as a function of time, where it can be observed that initial OCP is  $-12$  V, showing good stability in the NaOH aqueous solution under dark conditions after 40 s, stabilizing OCP at  $-14.5$  V, remaining almost constant. As reported by Huerta-Flores et al. [42], in the dark, OCP is controlled by

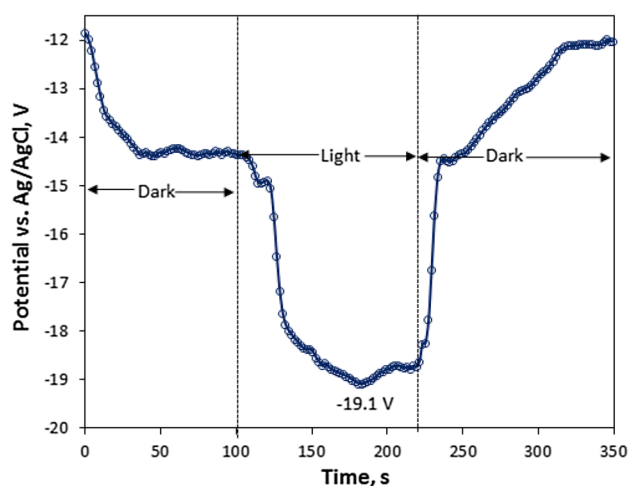


**Fig. 13** Illuminated OCP as a function of time under OFF/ON cycles of visible light illumination of ZnO/PPy electrode versus Ag/AgCl

interactions at the interface of solid composite film with the ionic solution and it is related to the particle size of composite. Under illumination, the OCP is shifted to more negative values indicating electrons accumulation in the conduction band, a typical behavior of n-type semiconductors [43], demonstrating the predominance of the ZnO nature over the p-type of PPy. After that, composite reached a maximum negative potential under illumination of  $-19.1$  V, and when illumination is OFF, the OCP value tends to potentials that are less negative, recovering until a value near to the initially observed in the dark. These results demonstrate a high electron–hole pair recombination.

## 4 Conclusions

The synthesized composite of ZnO/PPy consisting of rice-like ZnO nanoparticles dispersed in a semiconducting PPy matrix, showed high OII dye photodegradation efficiencies and fast reaction rates under the visible light irradiation. Almost 100% of photodegradation efficiency was achieved in only 30 min of visible light exposure at low initial dye concentration (10 mg/L) and a typical photocatalyst loading of 1.0 g/L. The observed photodegradation efficiencies and fast reaction were due to a synergistic interaction between semiconducting PPy and ZnO photocatalyst nanoparticles with a relatively low band gap energy of 3.05 eV. Hole and radical scavenger experiments allowed to conclude that  $\cdot\text{O}_2^-$  or ROS could be the main reactive species formed via reaction between  $\text{O}_2$  and photogenerated electrons at the surface of composite, following a pseudo-first order of reaction.

**Acknowledgements** V.M. Ovando-Medina acknowledges to CON-ACYT-México (Grant PDCPN-2015-384). Author M.P. Militello

acknowledges to Dr. V.M. Ovando-Medina for the hospitality during the post-doctoral leave in the Coordinación Académica Región Altiplano-UASLP (PRODEP-SEP #511-6/2019-13359/México, and CONICET/Argentina).

## Compliance with ethical standards

**Conflict of interest** On behalf of all authors, the corresponding author states that there is no conflict of interest.

## References

- Pereira, M. Alves, Environ. Prot. Strateg. Sustain. Dev. (2012). [https://doi.org/10.1007/978-94-007-1591-2\\_4](https://doi.org/10.1007/978-94-007-1591-2_4)
- P.A. Carneiro, R.F.P. Nogueira, M.V.B. Zanoni, Dye Pigment. (2006). <https://doi.org/10.1016/j.dyepig.2006.01.022>
- H. Zollinger, Leonardo (2006). <https://doi.org/10.2307/1575449>
- K.M. Ghanem, Afr. J. Microbiol. Res. (2012). <https://doi.org/10.5897/ajmr11.490>
- C. Greenhalgh, Endeavour (2004). [https://doi.org/10.1016/0160-9327\(77\)90195-8](https://doi.org/10.1016/0160-9327(77)90195-8)
- A. Pandey, P. Singh, L. Iyengar, Int. Biodeterior. Biodegrad. (2007). <https://doi.org/10.1016/j.ibiod.2006.08.006>
- T. Robinson, B. Chandran, P. Nigam, Enzyme Microb. Technol. (2001). [https://doi.org/10.1016/S0141-0229\(01\)00430-6](https://doi.org/10.1016/S0141-0229(01)00430-6)
- M. Riera-Torres, C. Gutiérrez-Bouzán, M. Crespi, Desalination (2010). <https://doi.org/10.1016/j.desal.2009.11.002>
- M. Ghaedi, B. Sadeghian, A.A. Pebdani, R. Sahraei, A. Daneshfar, C. Duran, Chem. Eng. J. (2012). <https://doi.org/10.1016/j.cej.2012.01.111>
- M.N. Chong, B. Jin, C.W.K. Chow, C. Saint, Water Res. (2010). <https://doi.org/10.1016/j.watres.2010.02.039>
- J. Kaur, S. Singhal, Ceram. Int. (2014). <https://doi.org/10.1016/j.ceramint.2013.12.088>
- S. Suleiman, N. Kaneva, A. Bojinova, K. Papazova, A. Apostolov, D. Dimitrov, Colloids Surf. A (2014). <https://doi.org/10.1016/j.colsurfa.2014.01.010>
- S. Bagheri, Z.A. Mohd Hir, A. Termeh Yousefi, S.B.A. Hamid, Microporous Mesoporous Mater. (2015). <https://doi.org/10.1016/j.micromeso.2015.05.028>
- H. Chaker, L. Chérif-Aouali, S. Khaoulani, A. Bengueddach, S. Fourmentin, J. Photochem. Photobiol. A (2016). <https://doi.org/10.1016/j.jphotochem.2015.11.025>
- I. Stambolova, M. Shipochka, V. Blaskov, A. Loukanov, S. Vassilev, J. Photochem. Photobiol. B (2012). <https://doi.org/10.1016/j.jphotobiol.2012.08.006>
- D. Wang, T. Xie, Y. Li, Nano Res. (2009). <https://doi.org/10.1007/s12274-009-9007-x>
- A. Umar, M.S. Chauhan, S. Chauhan, R. Kumar, G. Kumar, S.A. Al-Sayari, S.W. Hwang, A. Al-Hajry, J. Colloid Interface Sci. (2011). <https://doi.org/10.1016/j.jcis.2011.07.058>
- Z. Jin, Y.X. Zhang, F.L. Meng, Y. Jia, T. Luo, X.Y. Yu, J. Wang, J.H. Liu, X.J. Huang, J. Hazard. Mater. (2014). <https://doi.org/10.1016/j.jhazmat.2014.05.059>
- M. Zhong, Y. Li, I. Yamada, J.-J. Delaunay, Nanoscale (2012). <https://doi.org/10.1039/c2nr11451h>
- A. Hassanein, N. Salahuddin, A. Matsuda, G. Kawamura, M. Elfiky, Mater. Sci. Eng. C (2017). <https://doi.org/10.1016/j.msec.2017.04.101>
- F.M.A. Almuntaser, S. Majumder, P.K. Baviskar, J.V. Sali, B.R. Sankapal, Appl. Phys. A (2017). <https://doi.org/10.1007/s00339-017-1131-y>
- R. Kant, C. Dwivedi, S. Pathak, V. Dutta, Appl. Surf. Sci. (2018). <https://doi.org/10.1016/j.apsusc.2018.03.208>
- P.K. Chen, G.J. Lee, S.H. Davies, S.J. Masten, R. Amutha, J.J. Wu, Mater. Res. Bull. (2013). <https://doi.org/10.1016/j.materresbull.2013.02.062>
- Z. Mohd Hir, A. Abdullah, Z. Zainal, H. Lim, Catalysts (2017). <https://doi.org/10.3390/catal7110313>
- V.M. Ovando-Medina, L. Farías-Cepeda, N.V. Pérez-Aguilar, J. Rivera de la Rosa, H. Martínez-Gutiérrez, A. Romero Galarza, E. Cervantes-González, N. Cayetano-Castro, Rev. Mex. Ing. Quim. (2018). <https://doi.org/10.24275/uam/izt/dcbi/revmexingquim/2018v17n2/Ovando>
- D.A. González-Casamachin, J. Rivera De la Rosa, C.J. Lucio-Ortiz, D.A. De Haro De, D.X. Rio, G.A. Martínez-Vargas, N.E. Flores-Escamilla, V.M. Dávila, E. Moctezuma-Velazquez Ovando-Medina, Chem. Eng. J. (2019). <https://doi.org/10.1016/j.cej.2019.05.032>
- S. Yagi, S. Kobayashi, T. Inoue, T. Hori, N. Michiba, K. Okui, SAE Tech. Paper (2003). <https://doi.org/10.4271/2003-01-0987>
- J. Xie, Y. Li, W. Zhao, L. Bian, Y. Wei, Powder Technol. (2011). <https://doi.org/10.1016/j.powtec.2010.10.019>
- V.M. Ovando-Medina, R.G. López, B.E. Castillo-Reyes, P.A. Alonso-Dávila, H. Martínez-Gutiérrez, O. González-Ortega, L. Farías-Cepeda, Colloid Polym. Sci. (2015). <https://doi.org/10.1007/s00396-015-3717-2>
- E.R. García, R.L. Medina, M.M. Lozano, I.H. Pérez, M.J. Valero, A.M. Maubert Franco, Materials (Basel) (2014). <https://doi.org/10.3390/ma7128037>
- S. Anandan, Y. Ikuma, K. Niwa, Solid State Phenom. (2010). <https://doi.org/10.4028/www.scientific.net/ssp.162.239>
- F. Achouri, S. Corbel, L. Balan, K. Mozet, E. Giro, G. Medjahdi, M. Ben Said, A. Ghrabi, R. Schneider, Mater. Des. (2016). <https://doi.org/10.1016/j.matdes.2016.04.015>
- A. Benaboud, M. Zaabat, M.S. Aida, B. Boudine, S. Benzitouni, T. Saidani, Optik (Stuttg) (2017). <https://doi.org/10.1016/j.ijleo.2017.06.108>
- D. Zhang, F. Zeng, J. Iran. Chem. Soc. (2017). <https://doi.org/10.1007/s13738-017-1142-9>
- Z. Balta, E. Bilgin Simsek, D. Berek, Photochem. Photobiol. (2019). <https://doi.org/10.1111/php.13117>
- E. Bilgin Simsek, P. Demircivi, D. Berek, I. Novak, React. Kinet. Mech. Catal. (2018). <https://doi.org/10.1007/s11144-017-1320-x>
- P. Demircivi, E.B. Simsek, Water Sci. Technol. (2018). <https://doi.org/10.2166/wst.2018.298>
- F. Herrera, A. Lopez, G. Mascolo, P. Albers, J. Kiwi, Appl. Catal. B (2001). [https://doi.org/10.1016/S0926-3373\(00\)00198-3](https://doi.org/10.1016/S0926-3373(00)00198-3)
- S. Teixeira, P.M. Martins, S. Lanceros-Méndez, K. Kühn, G. Cuniberti, Appl. Surf. Sci. (2016). <https://doi.org/10.1016/j.apsusc.2016.05.073>
- Y. Liao, J. Brame, W. Que, Z. Xiu, H. Xie, Q. Li, M. Fabian, P.J. Alvarez, J. Hazard. Mater. (2013). <https://doi.org/10.1016/j.jhazmat.2013.05.047>
- D. Wang, Y. Wang, X. Li, Q. Luo, J. An, J. Yue, Catal. Commun. (2008). <https://doi.org/10.1016/j.catcom.2007.10.027>
- A.M. Huerta-Flores, I. Juárez-Ramírez, L.M. Torres-Martínez, J.E. Carrera-Crespo, T. Gómez-Bustamante, O. Sarabia-Ramos, J. Photochem. Photobiol. A (2018). <https://doi.org/10.1016/j.jphotochem.2017.12.029>
- D. Ramírez-Ortega, P. Acevedo-Peña, F. Tzompantzi, R. Arroyo, F. González, I. González, J. Mater. Sci. (2017). <https://doi.org/10.1007/s10853-016-0328-3>

**Publisher's Note** Springer Nature remains neutral with regard to jurisdictional claims in published maps and institutional affiliations.